

# Electrophysiological alterations of the Purkinje cells and deep cerebellar neurons in a mouse model of Alzheimer disease (electrophysiology on cerebellum of AD mice)

Guy Cheron<sup>1,2,3</sup>  | Dominique Ristori<sup>1</sup> | Javier Marquez-Ruiz<sup>4</sup> |  
Anna-Maria Cebolla<sup>1</sup>  | Laurence Ris<sup>3,5</sup> 

<sup>1</sup>Laboratory of Neurophysiology and Movement Biomechanics, Université Libre de Bruxelles, Brussels, Belgium

<sup>2</sup>ULB Neuroscience Institut, Université Libre de Bruxelles, Brussels, Belgium

<sup>3</sup>Laboratory of Neuroscience, Université de Mons, Mons, Belgium

<sup>4</sup>Department of Physiology, Anatomy and Cell Biology, Pablo de Olavide University, Seville, Spain

<sup>5</sup>UMONS Research Institut for health and technology, Université de Mons, Mons, Belgium

## Correspondence

Anna-Maria Cebolla, Laboratory of Neurophysiology and Movement Biomechanics, Université Libre de Bruxelles, Brussels, Belgium.  
Email: ana.maria.cebolla.alvarez@ulb.be

## Funding information

Fund of the Université de Mons; Leibniz Fund of the Université Libre de Bruxelles; the Belgian National Fund for Scientific Research (FNRS); the Brain and Society Foundation; the Queen Elisabeth Medical Foundation; Université Libre de Bruxelles

Edited by: Gianmaria Maccaferri

## Abstract

Alzheimer's disease is histopathologically well defined by the presence of amyloid deposits and tau-related neurofibrillary tangles in crucial regions of the brain. Interest is growing in revealing and determining possible pathological markers also in the cerebellum as its involvement in cognitive functions is now well supported. Despite the central position of the Purkinje cell in the cerebellum, its electrophysiological behaviour in mouse models of Alzheimer's disease is scarce in the literature. Our first aim was here to focus on the electrophysiological behaviour of the cerebellum in awake mouse model of Alzheimer's disease (APPswe/PSEN1dE9) and the related performance on the water-maze test classically used in behavioural studies. We found prevalent signs of electrophysiological alterations in both Purkinje cells and deep cerebellar nuclei neurons which might explain the behavioural deficits reported during the water-maze test. The alterations of neurons firing were accompanied by a dual (~16 and ~228 Hz) local field potential's oscillation in the Purkinje cell layer of Alzheimer's disease mice which was concomitant to an important increase of both the simple and the complex spikes. In addition,  $\beta$ -amyloid deposits were present in the molecular layer of the cerebellum. These results highlight the importance of the output firing modification of the AD cerebellum that may indirectly impact the activity of its subcortical and cortical targets.

## KEYWORDS

Alzheimer's disease, deep cerebellar nuclei, fast oscillation, inferior olive, mice, Purkinje cell

**Abbreviations:** AD, Alzheimer's disease; APP, amyloid precursor protein; A $\beta$ , amyloid-beta; CS, complex spike; CV, coefficient of variation; DCN, deep cerebellar nuclei; GFAP, glial fibrillary acidic protein; IBA1, ionized calcium-binding molecule 1; IO, inferior olive; ISI, interspike interval; LFP, local field potentials; LTD, long term depression; MWM, Morris Water Maze; PC, Purkinje cells; PFA, paraformaldehyde; p-tau, phospho-tau; RI, rhythm index; SS, simple spike; WT, wild type.

## 1 | INTRODUCTION

Alzheimer's disease (AD) is one of the most debilitating neurodegenerative pathologies of the aging brain, characterized by a progressive cognitive decline (Jacobs et al., 2018) and sometimes accompanied motor impairment (Bologna et al., 2020). AD is histopathologically defined by the presence of amyloid deposits and

tau-related neurofibrillary tangles, which are associated with loss of synapses and neurons in crucial regions of the brain (He et al., 2009; Ray & Buggia-Prevot, 2020; Yu et al., 2017). These histopathological traits are well identified with cerebrospinal biomarkers (i.e., amyloid-beta [ $A\beta$ ] and phospho-tau [p-tau] levels) (Canuet et al., 2015; Johnson et al., 2018; Mattsson et al., 2017).

Following a computationally relevant model, the brain may be considered as a dynamic recurrent network linking privileged connected nodes with hierarchical modularity (Braun et al., 2018; Stam, 2014) in which the cerebellum occupies a crucial position (de Zeeuw et al., 2020). The implication of the cerebellum in cognitive functions (Argyropoulos et al., 2020; Schmahmann, 2018) is supported by a well-studied recurrent network encompassing not only the olivo-cerebellar micromodules but also numerous subcortical and cortical regions relinked by long-range closed loops (Bostan & Strick, 2018; Caligiore et al., 2017; Fujita et al., 2020; Kelly & Strick, 2003).

Although the cerebellum has fewer  $A\beta$  deposits than the cerebral cortex (Baloyannis et al., 2000; Goedert, 2015) due to a more efficient  $A\beta$  drainage as demonstrated in the human APP knock-in AD mice model (Shahnur et al., 2020), recent studies (Baloyannis et al., 2016; Mavroudis, 2019; Mavroudis et al., 2013, 2019) have shown numerous pathological markers in the cerebellar cortex of AD patients. Amongst these, loss of dendritic spines and Purkinje cells (PC), synaptic alterations in the mossy fibres-granule cell dendrites and parallel fibres-PC dendrites explain the previously reported cerebellar atrophy and clinicopathological alterations (Wegiel et al., 1999). However, Singh-Bains et al. (2019) reported that the number of PC and tau immunoreactivity was unchanged in AD. In contrast, this study demonstrated significant changes in AD microglia (increased IBA1 expression and reduction of IBA1-positive cell process length and branching), confirming the multiple roles of microglia in the development of this pathology (Hansen et al., 2018).

Despite the volume of intense basic research, therapy and prevention of AD remain largely problematic and must be urgently reinforced (Johnson et al., 2018). From the most optimistic view, a definitive biological solution seems unattainable shortly. This burdensome situation calls for the promotion of a systematic perspective requiring the integration of multiregional brain data including the cerebellum. The human cerebellum represents almost 80% of the surface area of the neocortex (Serenio et al., 2020), so it can be viewed as a relevant entity in neurological disorders (Braun et al., 2018).

In this context, electrical oscillations are a key element of these networks dynamics and neural functions

(Buzsáki & Draguhn, 2004; Buzsáki & Watson, 2012; Giovanni et al., 2017; Watson & Buzsáki, 2015) in which the cerebellar oscillations can play a coordinating role (Cheron et al., 2004, 2016; Cheron, Márquez-Ruiz, et al., 2014; Courtemanche et al., 2013; Lévesque et al., 2020). Recent data support an integrative hypothesis where the cerebellum participates in the cognitive and neuropsychiatric deficits in AD (Jacobs et al., 2018; Kansal et al., 2017). Although the basic aspect of the physiology of the PC is central to understanding the influence of the cerebellum in AD, their main target neurons in the deep cerebellar nuclei (DCN), forming the only output of the cerebellum except for the vestibular-prepositus complex, need to be further explored. Besides its well-known role in motor learning, the cerebellum has a role in cognitive processes, such as spatial navigation during the formation of a hippocampal spatial map and during the induction of goal-directed behaviour (Mandolesi et al., 2001; Petrosini et al., 1996). A goal-oriented navigation task is a perfect example of a basic behavioural task involving most of the brain regions. It implies multimodal declarative learning (hippocampus) and procedural learning (basal ganglia) as well as task rules assimilation (prefrontal cortex) and sensorimotor adaptation (cerebellum). In this context, the cerebellum encoding body motion (Lefort et al., 2019; Rochefort et al., 2011) is thought to transform self-motion into goal-directed action, while the hippocampus codes for time and distance to allow path integration.

Here, we studied the consequences of the double mutation made on the APP<sup>swe</sup>/PSEN1<sup>dE9</sup> mice on the water-maze test classically used in behavioural studies involving not only the hippocampus but also the cerebellum (Rochefort et al., 2013). Despite the central position of the PC in the cerebellum, there is only one electrophysiological study (Huth et al., 2011) that examined the firing properties of the cerebellar neurons in mouse models of AD. To date, there are no published data about the electrophysiological behaviour of the cerebellum of the awake mouse model of AD. For this reason, our first aim was to study the firing discharge of the PC, the DCN neurons and the related local field potentials (LFP) in the APP<sup>swe</sup>/PSEN1<sup>dE9</sup> mice.

## 2 | METHODS

### 2.1 | Mice

APP<sup>swe</sup>/PSEN1<sup>dE9</sup> mice and wild type (WT) littermate control mice with the same SV129xC57Bl6 background aged 9 to 12 months, provided by Jackson Laboratory, USA, were used as experimental animals.

All animal procedures were approved by the University of Mons Ethical Committee and conducted following the European Union directive 609/86/EU. Every effort was made to minimize the number of animals and their discomfort. The present protocol used different cohorts of animals for the electrophysiology and the behavioural analysis.

## 2.2 | Surgical preparation

Animals were prepared for chronic recordings of local field potential (LFP) and PC single-unit activity. Mice were anaesthetized with xylido-dihydrothiazin (Rompun®, Bayer, 10 mg/kg) and ketamine (Ketalar®, Pfizer, 100 mg/kg). Animals were administered an additional dose of xylido-dihydrothiazin (3 mg/kg) and ketamine (30 mg/kg) when they demonstrated agitation or marked increases in respiration or heart rate during the procedure. Local anaesthesia (0.5 ml of 20 mg/ml lidocaine and adrenaline [1:80,000, Xylocaine®, Astra Zeneca]) was administered subcutaneously during the soft tissue removal. During surgery, two small bolts were cemented perpendicular to the skull to immobilize the head during the recording sessions, and a silver reference electrode was placed on the surface of the parietal cortex. To allow access to the vermis and the Crus I and II areas, and the deep nucleus in the cerebellum, an acrylic recording chamber was made around a posterior craniotomy (2 × 2 mm) and covered with a thin layer of bone wax (Ethicon®, Johnson & Johnson).

## 2.3 | Single-unit recordings in alert mice

Twenty-four hours after anaesthesia, alert mice were restrained for the recording session. The dura was removed over the cerebellum to expose the tissue in the recording chamber. Following the experimental evidence (Zhou et al., 2014) that the firing frequency of the PC simple spike (SS) in WT mice depends on their localization in zebrin<sup>+</sup> or zebrin<sup>-</sup> rostrocaudal bands, the specific recording place was kept in the same type of zebrin zone in both AD and WT control. The SS and complex spike (CS) recordings were thus performed in the PC layer of the lobule IV–V in zebrin<sup>-</sup>, and in the DCN, (interposed nucleus) following stereotaxic coordinates. The depths of the electrodes were also noted, and an electrolytic lesion was made 1 mm above the recording site (Figure 7e). To avoid unnecessary stress for the animals and movement artefacts, recording sessions were performed in a quiet room, when the animals were awake and calm. The alertness level was controlled by assessing

the maintenance of whisking activity during the recording session. We used quartz–platinum/tungsten microelectrodes (1.2–3 MΩ) in a seven-channel Eckhorn microdrive (Thomas Recordings®, Giessen, Germany). All measures of impedance were made with a 1 kHz sinusoidal current and checked throughout the recording session. In the present study, the exploration was made with one or two microelectrodes separated from 250 μm (outer and shaft diameters of 80 and 25 μm, respectively). The microelectrode was mounted into a stretched elastic rubber tube to enable proper positioning via DC-micromotors (resolution of 0.27 μm).

## 2.4 | Morris Water Maze

In parallel, eight mice of each genotype were used for behavioural analysis. During the learning phase, mice were placed four times per day from four different positions in the water maze (1.2 m of diameter) for four consecutive days. They had to reach an invisible platform placed just below the surface to escape the water in a maximal time of 2 min. The four different visual cues (3D geometrical shapes) were placed at cardinal points around the pool and were used by the mice for reference-based navigation. The time to reach the platform was measured at each trial and averaged during four consecutive days. On day 5, a retention test was performed by allowing the mice to navigate for 1.5 min in the water maze, while the platform was removed. The time spent in each quadrant was measured. All analyses were performed using the EthoVision XT software (Noldus, The Netherlands).

## 2.5 | Immunohistochemistry

Brains were fixed by 4% paraformaldehyde (PFA, pH 7.4, Sigma), dehydrated and embedded in a paraffin block for microtome sectioning in 5-μm thick sagittal sections.

Immunohistochemistry and haematoxylin staining were performed on two sections per animal ( $n = 24$  fields, four mice). For GFAP and immunofluorescence staining, sections were dewaxed, rehydrated and microwaved in 0.01 M sodium citrate buffer (pH 6.2, Sigma). Subsequently, the sections were incubated overnight at 4°C with a primary antibody: mouse monoclonal anti-GFAP 1:30 (glial fibrillary acidic protein, BD Biosciences, Cat# 556330, RRID: AB\_396368) for astrocytes, rabbit polyclonal anti-Iba1 1:150 (ionized calcium-binding molecule 1, Wako, Cat# 019-19741, RRID: AB\_839504) for microglia. The sections were then rinsed and incubated in the dark for 1 h with a fluorescent-conjugated

antibody diluted in blocking buffer: goat anti-mouse Alexa-Fluor 488 1:100 (Thermo Fisher Scientific, Cat# A11001, RRID: AB\_2534069) or goat anti-rabbit Alexa-Fluor 594 1:100 (Thermo Fisher Scientific, Cat# A11037, RRID: AB\_2534095). As a final step, the sections were rinsed (PBS, dH<sub>2</sub>O) and mounted with a Vectashield mounting medium containing DAPI (Vector Laboratories, USA).

For amyloid plaque detection and haematoxylin staining, after rehydration, sections were pre-treated with formic acid 70%, incubated overnight with anti-beta amyloid 17–24 antibody (4GB, Biologend, 1 µg/ml) and, after washing, incubated 1 h with HRP-goat anti-mouse antibody (4 µg/ml). Amyloid plaques were revealed by DAB/H<sub>2</sub>O<sub>2</sub>. Sections were then counterstained with haematoxylin and mounted. For quantitative analysis of GFAP and Iba1 immunostainings, the number of positive cells was counted in the cerebellum on 24 fields (0.1 mm<sup>2</sup>) per genotype.

## 2.6 | Data analysis and statistical methods

Neural activity signal recordings were filtered at 100 Hz high-pass and 10 kHz low-pass. LFP and single units were stored digitally on a computer after conversion with an analogue-digital converter (Power 1401, CED©, Cambridge, UK). The recorded data were digitized continuously at 20 kHz. Off-line analysis and illustrations were performed with Spike2 CED software (CED©). The rhythmic frequency was defined as the reciprocal of the latency of the first peak in the autocorrelogram of SS firing (width = 1 s, bin size = 1.0 ms). Consequently, the rhythmic frequency could not be determined on flat autocorrelograms. The strength of the rhythmicity was quantified with a rhythm index (RI) introduced by Sugihara et al. (1995). Briefly, peaks and valleys were recognized if their heights and depths exceeded the mean baseline level ± SD (measured at time lags of 250–300 ms). The RI was defined by the following formula:

$$RI = \frac{a1}{z} + \frac{b1}{z} + \frac{a2}{z} + \frac{b2}{z} + \dots,$$

in which  $a_i$  ( $i = 1, 2, \dots$ ) is the absolute value of the difference between the height of the  $i$ th peak and baseline level,  $b_i$  ( $i = 1, 2, \dots$ ) is the absolute value of the difference between the height of the  $i$ th valley and baseline level and  $z$  was the difference between the height of the zero-time bin and the baseline level. The regularity of the neuron was measured by the coefficient of variation (CV), defined as the quotient between the SD and the mean of

the frequency rate. The recording and analysis of the different neurons were made by an investigator blind mice genotype.

For statistical analysis of the behavioural data, two-way repeated-measures ANOVA was used to evaluate learning progression, followed by all Pairwise Multiple Comparison Procedures using the Holm-Sidak method. A two-way ANOVA was used to compare spatial strategy between WT and AD mice during learning and the memory retention test, followed by a Bonferroni post hoc test. For the counting of astrocytes and microglial cells, a Mann–Whitney rank-sum test was used. For the electrophysiological data, results are reported as mean ± SD and illustrated in box plots. The homogeneity and normality of the variances were checked by the Bartlett and Shapiro–Wilk test, respectively. Then parametric (t-test and ANOVA) or non-parametric (Wilcoxon rank-sum test with continuity correction) were applied for the comparative analysis between the AD and WT mice by using the software R version 4.03. The level of significance was set at  $p < 0.05$ .

## 3 | RESULTS

### 3.1 | Water-maze behaviour

Morris's water maze was used to evaluate spatial learning strategy and memory. Figure 1A illustrates the slower learning of AD mice and the increased time to reach the platform on the second day of training. Both wild-type (WT) and Alzheimer (AD) mice showed spatial learning ability as the time to reach the platform decreased significantly over time (two-way repeated-measures ANOVA, Holm-Sidak post hoc  $t$  test,  $p < 0.05$ ,  $n = 16$ ). However, a significant difference was observed in the learning phase of WT and AD mice. In WT mice, the time to reach the platform decreased from  $48.5 \pm 28.1$  s the first day to  $10.2 \pm 4.8$  s the second day and then remained constant over time. By contrast, in AD mice the decrease was slower starting from  $51.7 \pm 32.1$  s the first day, to reach  $29.8 \pm 15.4$  s the second day (which was significantly different from WT mice,  $t = 2.25$ ,  $p = 0.029$ ,  $n = 16$ ) and  $16.3 \pm 12.2$  the third day.

This slower learning could be explained by a different learning strategy used by AD mice compared to WT mice. Figure 1b shows that the percentage of time spent in the target quadrant (containing the platform) increased across days 1–3 in WT mice and was significantly higher than in AD mice (two-way ANOVA,  $t = 3.05$ ;  $p = 0.003$ ,  $n = 16$ ).

However, during the retention phase on day 5, when the platform was removed and the maze was divided into

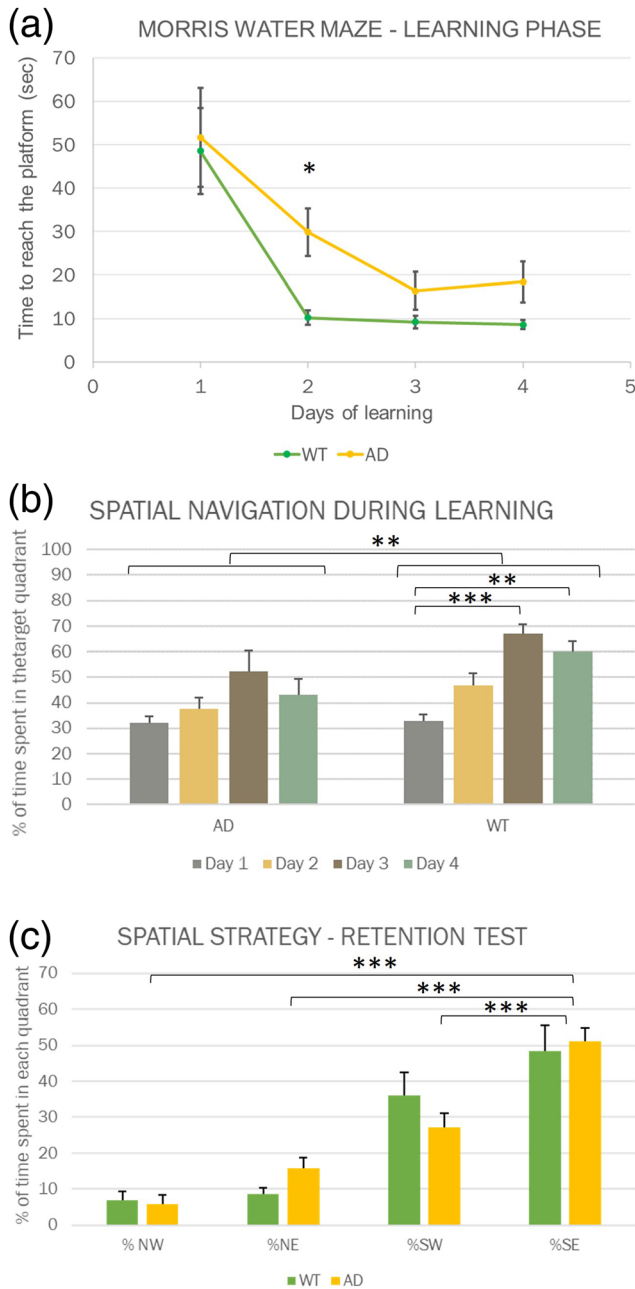


**FIGURE 1** (a) Learning phase in the Morris Water Maze. Both WT and AD mice (APP/PS1) demonstrated spatial learning ability, but AD mice took significantly more time to reach the platform on Day 2, ( $t = 2.25$ ;  $p = 0.029$ ,  $n = 16$ ). (b) Percentage of time spent in the target quadrant in AD and WT mice. WT mice spent significantly more time in the target quadrant than AD mice, two-way ANOVA ( $t = 3.05$ ;  $p = 0.003$ ,  $n = 16$ ) and WT mice increase the time spent in the target quadrant along with learning (Bonferroni post hoc test, Days 3 and 4 are different from Day 1,  $p < 0.001$ ,  $n = 16$ ). (c) During the retention test on Day 5, both WT and AD mice spent significantly more time in the SE quadrant where the platform was placed during the learning phase ( $p < 0.001$ ,  $n = 16$ ). The two groups are not different (two-way ANOVA,  $p = 1$ ). \*  $p < 0.05$ , \*\*  $p < 0.01$ , \*\*\*  $p < 0.001$

four quadrants (Figure 1c), AD mice showed a normal spatial strategy, passing more time in the fourth quadrant ( $51.2 \pm 10.6\%$  in AD mice compared  $48.5 \pm 18.9\%$ ) where the platform was originally placed (two-way ANOVA, Bonferroni post hoc test,  $p < 0.05$ ).

### 3.2 | Purkinje cells firing behaviour in AD mice

PC firing discharge is the sole output of the cerebellar cortex and one of the main inputs of the DCN neurons which firing discharge represents the final output of the cerebellum. Thus, we studied the spontaneous SS and CS PC firing, and DCN neurons in five (APPswe/PSEN1dE9) AD mice and six WT littermate control mice.

A total of 91 PCs were recorded (41 in AD and 50 WT mice). A representative PC firing in the AD mouse was illustrated in Figure 2 where it showed the two main types of firing mode (tonic, Figure 2a, and bursting, Figure 2b). As in WT mice, some PCs in AD mice may present the two modes during the recording session. However, whatever the mode of firing, the PCs recorded in AD mice presented a highly significant increase in the SS firing rate (Figure 3a) from  $72.3 \pm 28.8$  Hz in WT to  $145.9 \pm 65.8$  Hz in AD ( $p < 0.0001$ ,  $n = 91$ ). This increased firing was accompanied by a significant decrease of the CV from  $0.37 \pm 0.22$  in WT and  $0.16 \pm 0.07$  in AD ( $p < 0.0001$ ,  $n = 91$ ) (Figure 3b).

While the auto-correlogram of the SS firing was mainly flat in WT mice, it presented numerous side peaks in AD mice. This was illustrated in Figure 4 where the auto-correlogram of a representative AD PC showed slow (Figure 4a) and fast (Figure 4b) oscillations. Consequently, the rhythmicity index (RI) of the SS firing was significantly higher in AD mice, ( $0.04 \pm 0.053$  in WT vs.  $0.11 \pm 0.14$  in AD mice  $p < 0.009$ ,  $n = 91$ ) (Figure 3c). This significant change in the AD PC rhythmicity was also accompanied by the majority of recordings by a dual-frequency peak in the FFT profile of the LFP recorded in the PC layer of the AD mice (Figure 5c). The first peak corresponds to a slow oscillation at  $16.5 \pm 1.6$  Hz ( $n = 26$ ) and a faster one at  $228.7 \pm 22.9$  Hz ( $n = 31$ ). In some recordings, only the slow (beta) LFP oscillations were recorded (Figure 5a,b). The fast LFP oscillation was also present in WT mice at about the same frequency range ( $219 \pm 40.7$  Hz) but presented a very low peak amplitude ( $2.8 \times 10^{-5} \pm 2.0 \times 10^{-5} \mu V^2$ ) compared to the AD mice ( $1.5 \times 10^{-4} \pm 1.5 \times 10^{-4} \mu V^2$ ) (Figure 5d).

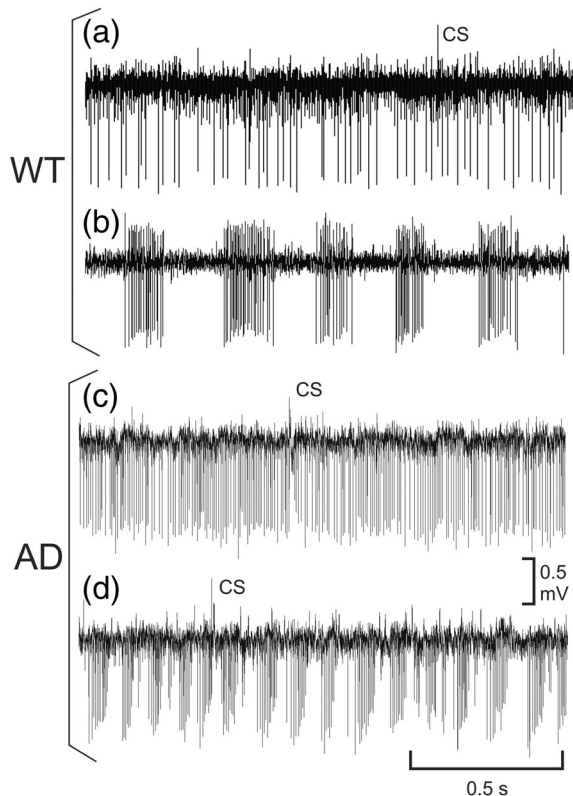


**FIGURE 2** Two modes of firing (tonic, a; bursting, b) of a Purkinje cell (extracellular recording) in an alert WT mouse and an AD mouse (tonic, c; phasic, d). Note the occurrence of the CS (less frequent event) into the more frequent SS

The CS firing frequency was doubled in AD mice (Figure 3d) from  $0.9 \pm 0.3$  Hz in WT to  $1.9 \pm 1.1$  Hz in AD ( $p < 0.0001$ ,  $n = 91$ ). The duration of the CS was decreased in AD mice from  $5.9 \pm 1.9$  ms in WT to  $4.6 \pm 2.0$  ms in AD ( $p < 0.002$ ,  $n = 91$ ) (Figure 3e). The duration of silence in the SS firing induced by the occurrence of the CS was decreased from  $6.3 \pm 2.8$  ms in WT mice to  $3.3 \pm 1.4$  ms in AD mice ( $p < 0.0001$ ,  $n = 91$ ) (Figure 3f). As previously demonstrated by Titley et al. (2019), the interspike interval (ISI) distribution of CS (Figure 6) illustrates the presence of CS clustering in WT mice (Figure 6b). This was reinforced in AD mice (Figure 6a). We found that 10.7% of CS (390 out of 3,653 CS) measured on 18 PC in 4 WT mice had an  $ISI \leq 200$  ms. This percentage increased in AD mice where 43.4% of CS (1,196 out of 2,752 CS) was measured in 14 PC in 4 AD mice. Statistical analysis with the Kruskal–Wallis chi-squared rank-sum test performed with 200 ms ISI bin demonstrated that these distributions were highly statistically different (Kruskal–Wallis = 96.091,  $df = 15$ ,  $p$  value =  $7.149e-14$ ,  $n = 6,405$ ). Namely, the Nonparametric Multiple Comparisons for relative contrast Estimation Method (Pairwise ranking) highlighted the significant increase of

the CS number in the first ISI interval of 200 ms (insert of Figure 6a) in the AD mice and contrast the significant increase of CS number in the 600 ms ISI interval in the WT mice (insert of Figure 6b).

### 3.3 | DCN neurons firing behaviour in AD mice

A total of 37 DCN neurons were recorded (18 in AD and 19 in WT mice). The firing of the DCN neurons in AD mice (Figure 7) presented a significant increase from  $48.2 \pm 20.1$  Hz in WT to  $68.0 \pm 31.7$  Hz in AD ( $p < 0.011$ ) (Figure 8a). This increase of firing was accompanied by a significant decrease of the CV from  $0.30 \pm 0.20$  in WT to  $0.20 \pm 0.10$  in AD ( $p < 0.014$ ,  $n = 37$ ) (Figure 8b). As for the PC, the RI of the DCN neurons was significantly increased from  $0.01 \pm 0.03$  in WT to  $0.18 \pm 0.23$  (Figure 8c).

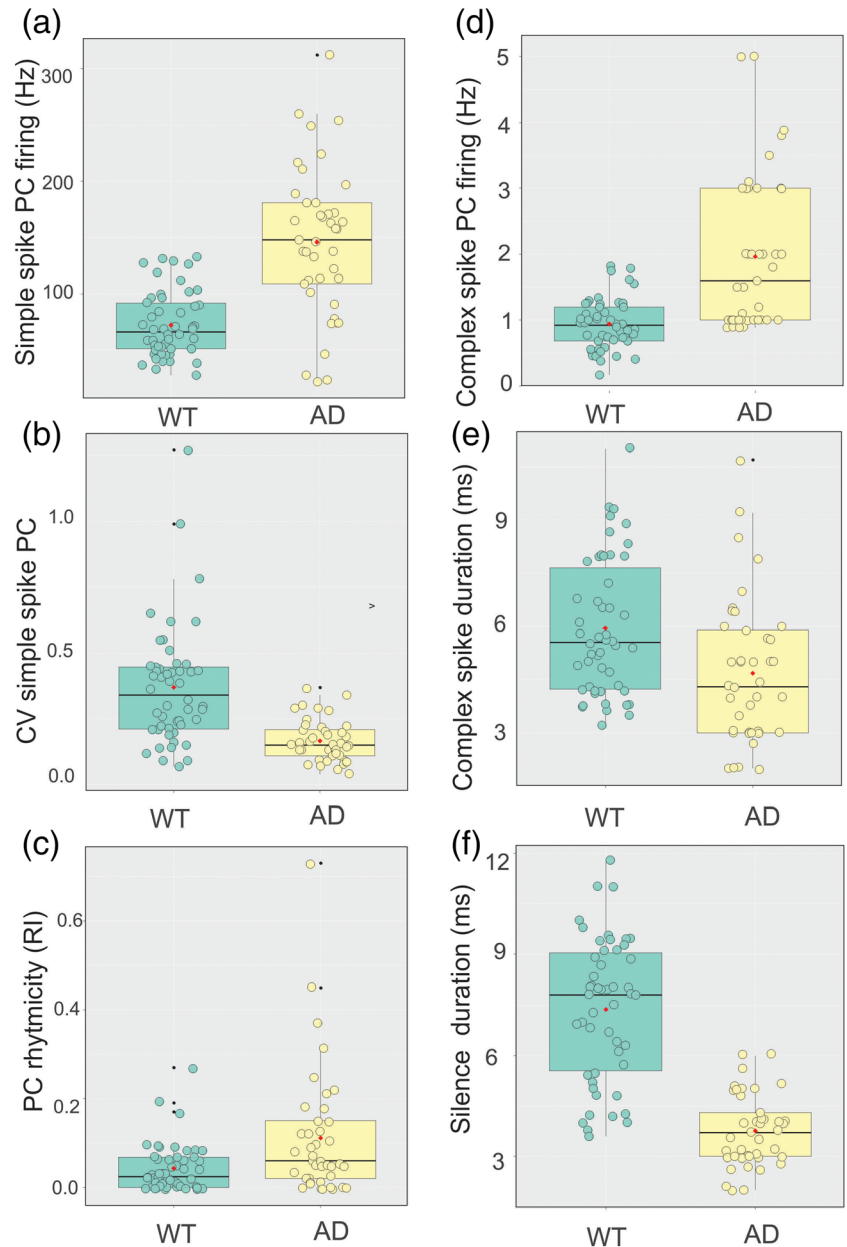
### 3.4 | Histological analysis of the cerebellum

The histological examination of cerebellar slices confirmed the presence of amyloid plaques deposits in the molecular layer but not in the other layers of the cerebellar cortex or the white matter (Figure 9a–c,f). The density of plaques was similar in the cerebellum and the cortex and hippocampus (Figure 9d) with a mean of  $1.37$  plaques/ $mm^2$  in the observed sections of AD mice ( $n = 4$ ), while no plaque was visible in WT mice (Figure 9e). In addition, the presence of gliosis was demonstrated in AD mice mainly in white matter but also in the molecular layer where plaques were observed (Figure 10) ( $n = 24$  fields, four mice). An increase of astrocytes and microglia density was revealed respectively by GFAP (Figure 10a–f) and IBA1 (Figure 10g,l) antibody, resulting in  $13.3 \pm 14.9$  astrocytes/ $mm^2$  in WT versus  $27.5 \pm 26.1$  in AD mice, ( $p < 0.05$ ,  $n = 24$ ) and  $7.1 \pm 9.5$  microglia/ $mm^2$  in WT versus  $24.6 \pm 20.0$ / $mm^2$  in AD (Mann–Whitney Rank Sum test,  $p < 0.001$ ,  $n = 24$ ).

## 4 | DISCUSSION

Three novel AD relevant findings emerge from this study. First, the behavioural analysis in the water maze demonstrated the presence of a learning deficit in the AD mice. Second, we identified significant signs of electrophysiological alterations in both PC and DCN neurons firing accompanied by a dual LFP oscillation in the PC layer of

**FIGURE 3** Boxplots representation of the firing frequency (a), the CV (b) and the rhythmicity index, RI (c) of the SS PC, and the CS firing (d), the CS duration (e) and the duration of the silence induced by the CS recorded in WT (green) and AD (yellow) mice. Boxes represent the inter-quartiles range (IQR) between the 25 (Q1) and 75 (Q3) percent quartiles, the horizontal lines inside the box indicate the median (Q2), the vertical lines mark the minimum (Q1–1.5\*IQR) and the maximum (Q3 + 1.5\*IQR); the red squares represent the mean and the black point the outliers data. Note the significant increase of the SS frequency ( $p < 0.0001$ ,  $n = 91$ ) and the large dispersion of the dataset (a) and the presence of one outlier in AD mice. A reverse situation is observed for the CV (b) presenting a significant decrease ( $p < 0.0001$ ,  $n = 91$ ) and a reduced dispersion of the dataset in AD. The significant increase of the RI ( $p < 0.009$ ,  $n = 91$ ) in the AD mice (c) is also accompanied by a larger dispersion



these AD mice. Finally, these behavioural and electrophysiological alterations were accompanied by the presence of  $\beta$ -amyloid deposits in the molecular layer of the cerebellum, paralleling findings in the hippocampus and by an increase in the number of astrocytes and activated microglial cells.

#### 4.1 | Discussion of the learning deficit

Spatial navigation is impaired in AD patients, even at preclinical stages (Allison et al., 2016). Animal models of AD expressing mutated APP or double transgenic for APP and PS1 also showed impairment in spatial navigation evaluated in the cued or reference memory version

of the Morris Water Maze (MWM). Zhao et al. (2014) demonstrated that mice expressing humanized APP bearing two mutations learned more slowly in the MWM and were less performant in the 24 h recall test. This impairment was observed at 11 months of age when a high amyloid load was observed in the hippocampus and cortex. In male heterozygous APP<sup>sw</sup>/PS1 mice, Bergin et al. (2018) presented evidence of impairment in the reference memory version of MWM at 13 months but not at 7 months; the older mice presented more thigmotaxis indicating a non-spatial learning strategy. Similarly, Chen et al. (2000) showed that PDAPP mice were impaired in spatial navigation in an age-dependent manner, concerning soluble and insoluble amyloid load in the hippocampus.

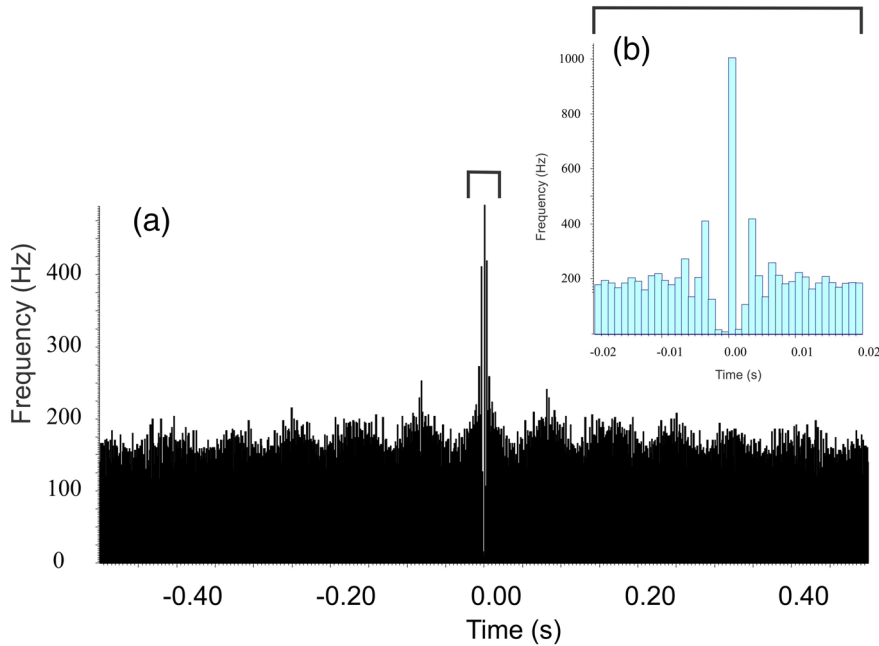


**FIGURE 4** Auto-correlogram of the SS firing of a representative PC in an AD mouse showing the slow oscillation (12.5 Hz) (a) and the fast oscillation (257 Hz) in the central magnification part of the auto-correlogram (b)

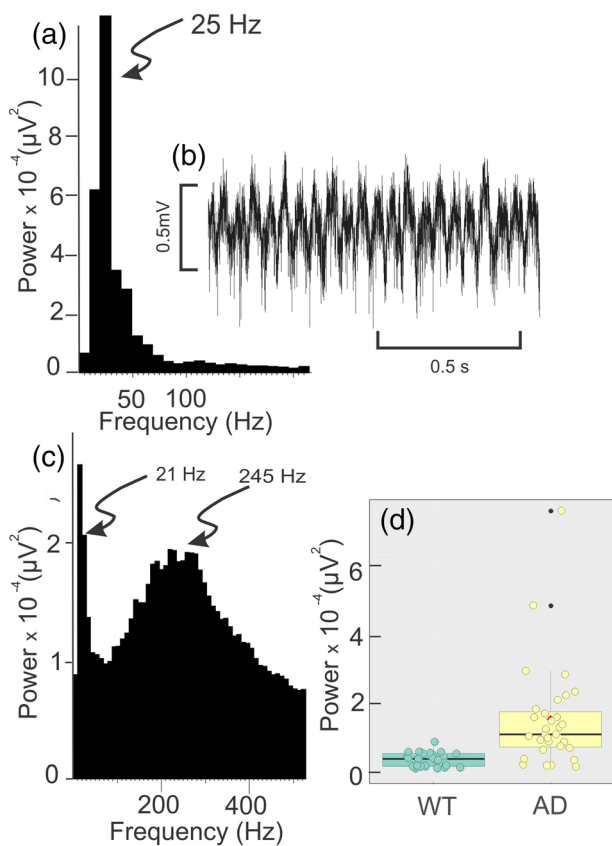


**FIGURE 5** Example of a beta LFP oscillation (25 Hz) FFT histogram (a), raw LFP recording (b) and a dual-frequency LFP oscillation (c) (21 and 245 Hz) recorded in the PC layer of AD mouse. Boxplot representation of the LFP power in WT (green) and AD (yellow) mice

Interestingly, Ordóñez-Gutiérrez et al. (2015) and Cayzac et al. (2015) showed that before any sign of behavioural deficit, 6-month-old APP/PS1 mice presented alteration of local oscillatory activity in the hippocampus and inflexible hippocampal representation of space during learning tasks. In a more recent study, Chen et al. (2021) demonstrated that 9- to 12-month-old APP/PS1 mice presented alteration in hippocampal sharp-wave ripples during sleep concerning myelin loss in cortex, hippocampus and corpus callosum suggesting network activity dysregulation.

Our results demonstrating alteration of the electrical activity of Purkinje and DCN cells suggest that cerebellar dysfunction could add up to hippocampal-related behavioural deficit. Spatial navigation of the L7-PKC1 mutant mice showed that the cerebellum was more specifically involved in goal-directed navigation, suggesting that cerebellar representation of the body in space could help to construct the hippocampal place fields during spatial navigation (Passot et al., 2012; Rochefort et al., 2013). This important role of the cerebellum in the acquisition phase of MWM was confirmed in hemicerebellectomized rats (Petrosini et al., 1996) which were unable to develop efficient searching behaviour during the acquisition phase while being able to use place strategy after cue-dependant learning. In the same line of evidence, lesion of the ponto or olivo-cerebellar pathway (Gasbarri et al., 2003) altered the learning phase of the spatial task as well as the retention phase while more specific dentate nucleus lesion did not alter MWM performance (Gaytán-Tocavén & Olvera-Cortés, 2004).

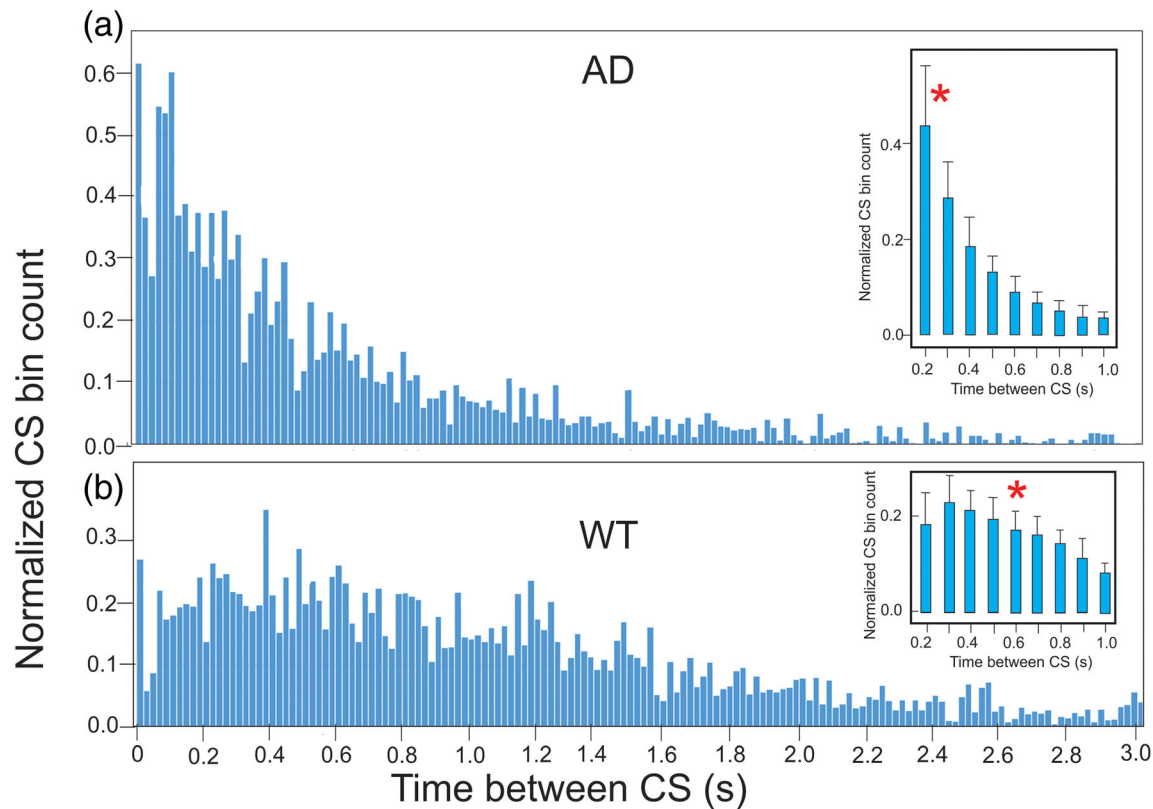


**FIGURE 6** Histograms of spontaneous CS interspike intervals in 20 ms bins in AD (a) and WT (b) mice. These distributions were performed on a total time of 5 s, but only the first 3 s is illustrated. The CS bin count is normalized. The insert illustrates the statistical analysis (Kruskal–Wallis chi-squared rank-sum test) performed on 200 ms bins in which the asterisk highlighted the significant difference ( $p < 0.0001$ ,  $n = 6,405$ )

## 4.2 | Increased SS and CS firing

Although the SS firing is influenced by both intrinsic factors (Raman et al., 2000; Raman & Bean, 1997) and synaptic modulation (Cheron, Prigogine, et al., 2014; Servais & Cheron, 2005; de Zeeuw et al., 2011), Zhou et al. (2014) demonstrated that it also depends on the PC localization in zebrin<sup>+</sup> or zebrin<sup>-</sup>. As the present recordings were specifically realized in the same cerebellar region (lobules IV–V) corresponding in majority to a zebrin<sup>-</sup>, the increased firing reported in the AD mice was not biased by a change in zebrin type. Indeed, the PC's firing recorded in the present WT mice ( $75.8 \pm 19.5$  Hz) was very similar that the one ( $72.3 \pm 28.8$  Hz) reported in the zebrin<sup>-</sup> by Zhou et al. (2014), which contrasts to the frequency recorded in zebrin<sup>+</sup> ( $36.0 \pm 15.5$  Hz) in this later study. Accordingly, the zebrin-type bias can be excluded on the CV of the SS firing which was situated about 0.4 units in both Zhou et al. (2014) study, and in our present WT mice sample. We can thus assume that the significant CV reduction in AD mice (0.16) was not due to the zebrin<sup>-</sup> versus zebrin<sup>+</sup>. In spite that the frequency of the CS firing was also

zebrin zone dependent, the significant frequency increase in AD mice cannot be explained by the recording in the Z<sup>+</sup> zone for which a slower frequency rate has been reported in WT mice (Zhou et al., 2014).

One possible explanation of the huge increase in the SS firing could be related to the increased activity of the  $\beta$ -secretase BACE1 in AD (Huth et al., 2011; Kim et al., 2007; Kovacs et al., 2010). This protease is a key enzyme initiating not only the formation of the A $\beta$  plaques (Vassar et al., 1999) but also facilitates the activity of the resurgent Na<sup>(+)</sup> current (INaR) of the PC (Huth et al., 2011). It was demonstrated in histological preparation that the INaR decay was significantly faster in BACE1-deficient PC than in WT cells producing a slower firing rate of the Purkinje cell. Conversely, increased BACE1 activity in AD could explain the present firing increase of the PC in AD mice.

The increased CS firing could be understood following the classical closed-loop model linking the inhibitory PC input to the GABAergic DCN neurons projecting to the IO (GAD + IO). The PC hyperactivity may potentially induce disinhibition of the IO neurons which in turn produce the increase of the climbing fibre activity

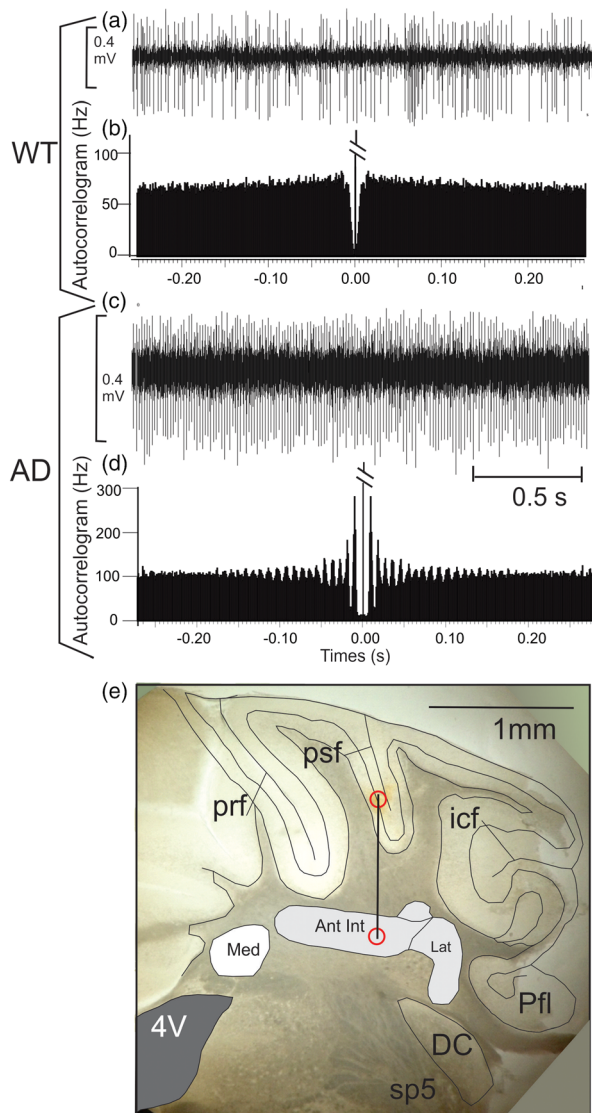


**FIGURE 7** Extracellular recording of representative DCN neuron in an alert WT (a, b) and AD mouse (c, d), respectively. Note the higher frequency rate and the numerous side peak in AD mice. (e) Photograph of a brain slice passing through a recording tract showing the electrolytic lesion performed 1 mm above (upper red circle) the region of interest in the interposed DCN (lower red circle). The slice corresponds to the Bregma -6 mm. Abbreviation: 4V, fourth ventricle; sp5, spinal trigeminal tract; DC, dorsal cochlear nucleus; Pfl, paraflocculus; Med, fastigial nucleus; Ant int, anterior interposed nucleus; Lat, dentate nucleus; icf, intercrural fissure; psf, post superior fissure; prf, primary fissure. The vertical line corresponds to the tract

and related CS firing increase. However, the disinhibition of the IO neurons does not seem to reconcile the fact that we found an increased, not decreased firing of the present recorded DCN neurons. It could be argued that we did not record the GABAergic (GAD67-positive, GAD + IO) neurons (Uusisaari & Knöpfel, 2008) as these

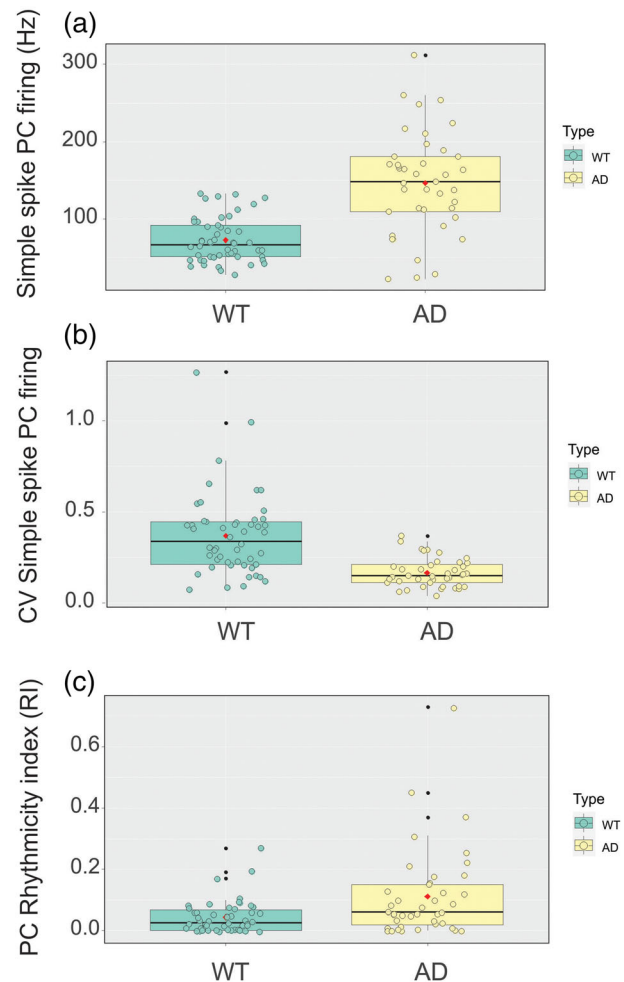


**FIGURE 8** Boxplots representation of the firing frequency (a), the CV (b) and the rhythmicity index, RI (c) of the DCN neurons recorded in WT and AD mice. The same boxplot illustration as in Figure 3 is used. Note the significant increase of the DCN neuron frequency ( $p < 0.011$ ): (a) the reduction of the CV ( $p < 0.014$ ,  $n = 37$ ) and (b) the important increase of the RI ( $p < 0.001$ ,  $n = 37$ ) (c) in AD mice

neurons are smaller than the glutamatergic projecting neurons and more difficult to be recorded in alert mice. However, the increased firing of the other non-GABAergic DCN neurons could be explained by an increased excitatory input from the climbing fibre collaterals which overcompensate for the increased inhibition provided by the PC (Cheron & Cheron, 2018). All in all, the possibility that these DCN neurons (GAD + IO) which are implicated in the functional loop linking the cerebellar cortex, the DCN and the IO (Ruigrok & Teune, 2014) were more inhibited by the increased PC firing remains open and must be specifically examined in future studies.

Concerning the firing increase of the CS in AD mice, the recent study of Titley et al. (2019) pointed to

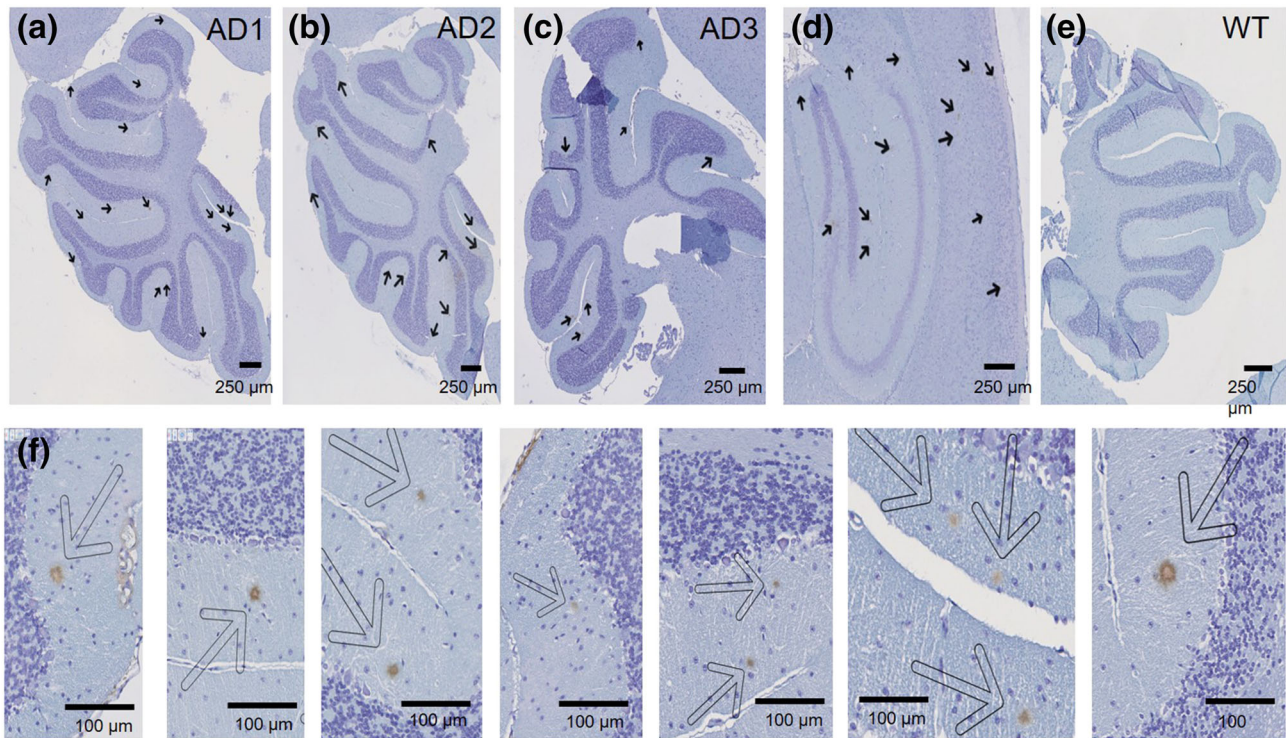


**FIGURE 9** Immunohistological analyses of the cerebellar slices. (a–e) Amyloid plaques (arrows) detected by anti-beta-amyloid 17–24 antibody (4G8, Biologend, 1 μg/ml) are visible in the molecular layer of the cerebellum (a–c) and the hippocampus (d) of AD mice (APP/PS1), but not in the cerebellum of WT mice (e). Scale bar: 250 μm. (f) Examples of amyloid plaques observed at higher magnification. Scale bar 100 μm

the existence of a CS clustering in WT mice occurring when the ISI interval was shorter than 100 ms. The fact that we found a significant increase of this CS clustering in AD mice reinforced the idea that during sensory stimulation in WT animals (Bosman et al., 2010; Márquez-Ruiz & Cheron, 2012) the IO of AD mice are over-excited, potentially increasing the probability to produce doublet CS.

Another explanation could come from the alteration of the intrinsic mechanism controlling subthreshold IO oscillations (Leznik & Llinás, 2005; Llinás, 2013; Llinás et al., 1974) which may explain the present hyperexcitability of the IO of AD mice. Interestingly, a significant loss of IO neurons (34%) and oligodendrocytes (46%) has been reported in human AD (Lasn et al., 2001, 2006) which could induce functional reinnervation with new sprouting olivary axons (inducing increased CS) terminating around the proximal dendrites of Purkinje cells (Rossi et al., 1991). Also, in one aged patient with mild cognitive impairment, diffuse spongiform changes were reported in the IO (Fernández-Vega et al., 2015) accompanied by immunocytochemical alterations, indicating that the intrinsic mechanisms at the basis of the climbing fibre activation could explain an increase of the CS firing.

### 4.3 | Dual-frequency LFP oscillation and a vicious circle

The fact that the dual-frequency (~16 and ~228 Hz) LFP oscillation was concomitant with an important increase of both the SS and the CS, firing may be explained by abnormal neuronal hyperactivity in this part of the cerebellar cortex and by hyperactivity of the IO output.

As presently demonstrated in our mouse model, this pathological state was accompanied by the presence of β-amyloid deposits in the molecular layer of the cerebellum. A similar vicious circle has been described in the hippocampus (Zott et al., 2019) between the presence of β-amyloid deposits and neuronal hyperactivation due to a lack of recovery of the glutamate reuptake. This alteration of glutamate reuptake was also discovered in the cerebellar PC of awake heterozygous *Glt1<sup>-/+</sup>* and *DMXL* mice (Sicot et al., 2017) where an important increase of the LFP ~200 Hz oscillation in the PC layer was reported as in the present AD mice.

The recent models of Zang et al. (2020) verified the fact that in the present AD mice, the LFP power recorded in the PC layer occurred in the presence of an increase of the PC firing rate. However, this has not been always reported in other pathological mouse models

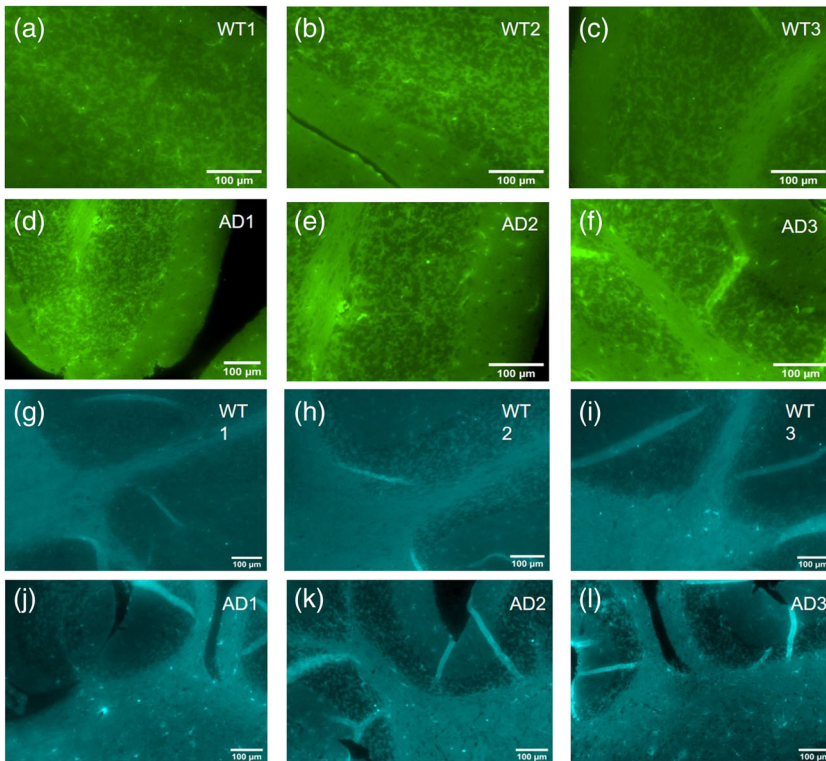
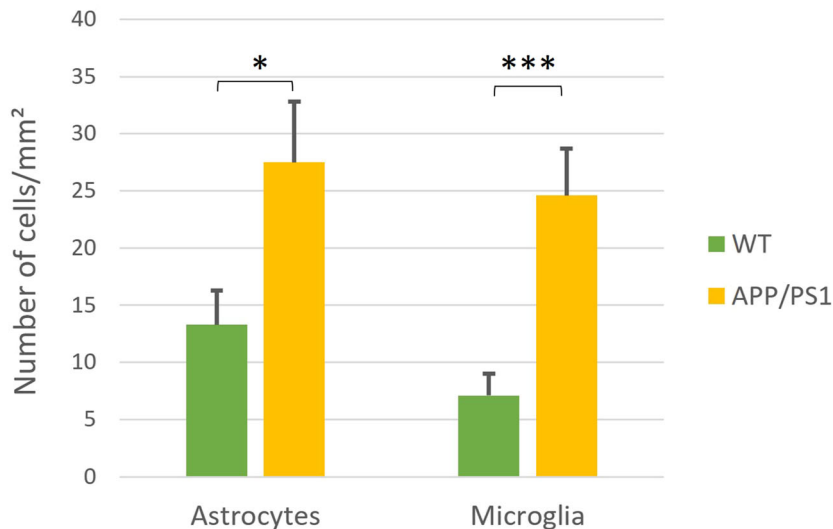


**FIGURE 10** Immunohistological analyses of gliosis in the cerebellar slice of AD mice (APP/PS1) (d–f; j–l) compared to WT mice (a–c; g–h). Astrocytes are observed in the white matter and the molecular layer of the cerebellum (a–f) while microglial cells are mainly observed in the white matter (g–l). Scale bar: 100  $\mu\text{m}$ . The graph represents the mean number of astrocytes and microglial cells per  $\text{mm}^2$  in WT and AD mice ( $n = 24$  fields, 4 mice), Mann–Whitney rank sum test, \*  $p < 0.05$ , \*\*\*  $p < 0.001$



( $PV^{-/-}CB^{-/-}$  (Servais et al., 2005);  $BK^{-/-}$  (Cheron et al., 2009) and  $PC-BK^{-/-}$  (Cheron et al., 2018) in which high LFP powers were recorded while the firing frequency of the PC was significantly decreased. Besides, dual-frequency oscillations were also reported in these later mutants, also presenting higher RI, but that without the present increase of SS firing in the AD mice. The increase of the RI in both PC and DCN neurons in AD mice could be discussed in comparison to a similar RI increase in  $PC-BK^{-/-}$  in which only the genetic alteration (suppression of the BK channels) in PC induced a huge increase of the PC rhythmicity (RI). In this case, the

increased RI of the PC was induced by the emergence of a beta burst of PC firing, which produced a reciprocal bursting in the firing of the DCN neurons. Following Person and Raman (2011), it was concluded that rhythmic alteration of the PC can be transmitted to the DCN neurons (Cheron et al., 2018). This may partially explain the present RI increase of the DCN neurons in AD mice, but the presence of pathology (vicious circle) linked to neuroinflammation and plaques in the DCN must be taken into account in further studies. Interestingly, a recent fMRI study (Olivito et al., 2020) has revealed a hyperconnectivity between the DCN and

temporo-occipital cortex suggesting an increased neural synchronization between the cerebellum and these cortical areas in AD patients. It could be possible that this synchrony increase was potentiated by a more rhythmic output of the DCN as reported in the present AD mice.

#### 4.4 | Histological alterations in AD human versus mice

Even though the human cerebellum presented no neurofibrillary changes, diffuse neuritic plaques (Baloyannis et al., 2016; Catafau et al., 2016; Mavroudis et al., 2010, 2013, 2019) and morphological alterations of the cerebellum have been well recognized and characterized by atrophy in the anterior cerebellar lobe (Mavroudis, 2019). Besides, the PC density on the vermis and hemispheres was significantly decreased, accompanied by a loss of their secondary and tertiary dendritic arborization and a significant decrease of the dendritic spines density (Mavroudis et al., 2010). Morphological analysis in the cerebellar nodulus and flocculus (Baloyannis et al., 2000) also demonstrated a significant loss of granule and Golgi cells accompanied by a decrease of the synapses between the mossy fibers and the dendrites of the granule and Golgi cells.

Recently, Massimi et al. (2020) revisited the underestimated presence of amyloid deposit in the cerebellum of APP/PS1 transgenic mice and demonstrated the presence of elongated plaques similar to the ones found in AD humans. As in the present AD mutant, these plaques are specifically concentrated in the molecular layer and generally absent in the other layers of the cerebellar cortex.

In our study, 9 to 12 months old mice presented a low number of amyloid plaques in the hippocampus, which could explain the mild deficit observed in MWM test. The same density of amyloid plaques was observed in the molecular layer of the cerebellum, in agreement with previous findings in the same mouse model. Indeed, plaque deposition in the cerebellum has been demonstrated to be age and sex-dependent (Ordoñez-Gutiérrez et al., 2015, 2016).

Moreover, Chang et al. (2019) revealed extensive metabolic alterations in the cerebellum of APP/PS1 mice. As neuroinflammation is a well-recognized hallmark in AD, the importance of the molecular mechanisms linking neuroinflammation and plaque formation has been studied by the quantification of the S100 proteins family in the APP23 mice (Hagmeyer et al., 2019). These authors reported that the proinflammatory S100B protein is highly expressed in

the PC and that S100B, S100A6 and S100A8 proteins are co-localized with A $\beta$  plaques. In the present situation, gliosis was observed mainly in the white matter of the cerebellum indicating that the alterations due to amyloid plaque deposit and those linked to microglia activation concern two different regions of the cerebellum (white matter and molecular layer) but spare the granular layer.

Finally, the present electrophysiological alterations of the PC and the DCN neurons may explain the behavioural deficits reported during the water-maze test as in cerebellar LTD deficient mice (Rocheffort et al., 2013). These results highlight the importance of the output firing modification of the AD cerebellum that may indirectly impact the activity of its subcortical and cortical targets.

#### ACKNOWLEDGEMENTS

The authors thank T.D'Angelo, M. Dufief, E. Hortmanns, M. Petieau, E. Toussaint for expert technical assistance, Scott Mongold for English proofreading, the Queen Elisabeth Medical Foundation, the Belgian National Fund for Scientific Research (FNRS), the Brain and Society Foundation, and the Leibniz Fund of the Université Libre de Bruxelles and the Fund of the Université de Mons (Belgium).

#### CONFLICT OF INTEREST

The authors declare that they have no known competing financial interests or personal relationships that could have appeared to influence the work reported in this paper.

#### AUTHOR CONTRIBUTIONS

G.C. and R.L. conceived the original idea. G. C, R.L. and J.M.R. designed the experiment. G.C., R.L. and A.M.C. performed the experiments. G.C. and D.R. performed the data analysis. G.C. and R.L. wrote the paper. J.M.R. and A.M.C. contributed to the writing.

#### PEER REVIEW

The peer review history for this article is available at <https://publons.com/publon/10.1111/ejn.15621>.

#### DATA AVAILABILITY STATEMENT

All relevant data will be available from the corresponding authors upon request.

#### ORCID

Guy Cheron  <https://orcid.org/0000-0003-0734-583X>  
 Anna-Maria Cebolla  <https://orcid.org/0000-0002-3710-7923>  
 Laurence Ris  <https://orcid.org/0000-0002-2140-8297>

## REFERENCES

- Allison, S. L., Fagan, A. M., Morris, J. C., & Head, D. (2016). Spatial navigation in preclinical Alzheimer's disease. *Journal of Alzheimer's Disease*, *52*, 77–90.
- Argyropoulos, G. P. D., van Dun, K., Adamaszek, M., Leggio, M., Manto, M., Masciullo, M., Molinari, M., Stoodley, C. J., van Overwalle, F., Ivry, R. B., & Schmahmann, J. D. (2020). The cerebellar cognitive affective/Schmahmann syndrome: A task force paper. *Cerebellum London England*, *19*, 102–125.
- Baloyannis, S. J., Manolidis, S. L., & Manolidis, L. S. (2000). Synaptic alterations in the vestibulocerebellar system in Alzheimer's disease—A Golgi and electron microscope study. *Acta Otolaryngol (Stockh)*, *120*, 247–250.
- Baloyannis, S. J., Mavroudis, I., Baloyannis, I. S., & Costa, V. G. (2016). Mammillary bodies in Alzheimer's disease: A Golgi and electron microscope study. *American Journal of Alzheimer's Disease and Other Dementias*, *31*, 247–256.
- Bergin, D. H., Jing, Y., Mockett, B. G., Zhang, H., Abraham, W. C., & Liu, P. (2018). Altered plasma arginine metabolome precedes behavioural and brain arginine metabolomic profile changes in the APP<sup>swe</sup>/PS1 $\Delta$ E9 mouse model of Alzheimer's disease. *Translational Psychiatry*, *8*, 108.
- Bologna, M., Guerra, A., Colella, D., Cioffi, E., Paparella, G., di Vita, A., D'Antonio, F., Trebbastoni, A., & Berardelli, A. (2020). Bradykinesia in Alzheimer's disease and its neurophysiological substrates. *Clinical Neurophysiology*, *131*, 850–858.
- Bosman, L. W. J., Koekkoek, S. K. E., Shapiro, J., Rijken, B. F. M., Zandstra, F., van der Ende, B., Owens, C. B., Potters, J.-W., de Grijl, J. R., Ruigrok, T. J. H., & de Zeeuw, C. I. (2010). Encoding of whisker input by cerebellar Purkinje cells. *The Journal of Physiology*, *588*, 3757–3783.
- Bostan, A. C., & Strick, P. L. (2018). The basal ganglia and the cerebellum: Nodes in an integrated network. *Nature Reviews Neuroscience*, *19*, 338–350.
- Braun, U., Schaefer, A., Betzel, R. F., Tost, H., Meyer-Lindenberg, A., & Bassett, D. S. (2018). From maps to multi-dimensional network mechanisms of mental disorders. *Neuron*, *97*, 14–31.
- Buzsáki, G., & Draguhn, A. (2004). Neuronal oscillations in cortical networks. *Science*, *304*, 1926–1929.
- Buzsáki, G., & Watson, B. O. (2012). Brain rhythms and neural syntax: Implications for efficient coding of cognitive content and neuropsychiatric disease. *Dialogues in Clinical Neuroscience*, *14*, 345–367.
- Caligiore, D., Pezzulo, G., Baldassarre, G., Bostan, A. C., Strick, P. L., Doya, K., Helmich, R. C., Dirx, M., Houk, J., Jörntell, H., Lago-Rodríguez, A., Galea, J. M., Miall, R. C., Popa, T., Kishore, A., Verschure, P. F. M. J., Zucca, R., & Herrerros, I. (2017). Consensus paper: Towards a systems-level view of cerebellar function: The interplay between cerebellum, basal ganglia, and cortex. *Cerebellum London England*, *16*, 203–229.
- Canuet, L., Pusil, S., López, M. E., Bajo, R., Pineda-Pardo, J. Á., Cuesta, P., Gálvez, G., Gaztelu, J. M., Lourido, D., García-Ribas, G., & Maestú, F. (2015). Network disruption and cerebrospinal fluid amyloid-beta and phospho-tau levels in mild cognitive impairment. *Journal of Neuroscience: The Official Journal of the Society for Neuroscience*, *35*, 10325–10330.
- Catafau, A. M., Bullich, S., Seibyl, J. P., Barthel, H., Ghetti, B., Leverenz, J., Ironside, J. W., Schulz-Schaeffer, W. J., Hoffmann, A., & Sabri, O. (2016). Cerebellar amyloid- $\beta$  plaques: How frequent are they, and do they influence 18F-Florbetaben SUV ratios? *Journal of Nuclear Medicine*, *57*, 1740–1745.
- Cayzac, S., Mons, N., Ginguay, A., Allinquant, B., Jeantet, Y., & Cho, Y. H. (2015). Altered hippocampal information coding and network synchrony in APP-PS1 mice. *Neurobiology of Aging*, *36*, 3200–3213.
- Chang, K. L., Wong, L. R., Pee, H. N., Yang, S., & Ho, P. C.-L. (2019). Reverting metabolic dysfunction in cortex and cerebellum of APP/PS1 mice, a model for Alzheimer's disease by pioglitazone, a peroxisome proliferator-activated receptor gamma (PPAR $\gamma$ ) agonist. *Molecular Neurobiology*, *56*, 7267–7283.
- Chen, G., Chen, K. S., Knox, J., Inglis, J., Bernard, A., Martin, S. J., Justice, A., McConlogue, L., Games, D., Freedman, S. B., & Morris, R. G. (2000). A learning deficit related to age and beta-amyloid plaques in a mouse model of Alzheimer's disease. *Nature*, *408*, 975–979.
- Chen, L., Zhou, Y.-P., Liu, H.-Y., Gu, J.-H., Zhou, X.-F., & Yue-Qin, Z. (2021). Long-term oral administration of hyperoside ameliorates AD-related neuropathology and improves cognitive impairment in APP/PS1 transgenic mice. *Neurochemistry International*, *151*, 105196.
- Cheron, G., Gall, D., Servais, L., Dan, B., Maex, R., & Schiffmann, S. N. (2004). Inactivation of calcium-binding protein genes induces 160 Hz oscillations in the cerebellar cortex of alert mice. *Journal of Neuroscience: The Official Journal of the Society for Neuroscience*, *24*, 434–441.
- Cheron, G., Márquez-Ruiz, J., Cheron, J., Prigogine, C., Ammann, C., Lukowski, R., Ruth, P., & Dan, B. (2018). Purkinje cell BKchannel ablation induces abnormal rhythm in deep cerebellar nuclei and prevents LTD. *Scientific Reports*, *8*, 4220–4237.
- Cheron, G., Márquez-Ruiz, J., & Dan, B. (2016). Oscillations, timing, plasticity, and learning in the cerebellum. *Cerebellum London England*, *15*, 122–138.
- Cheron, G., Márquez-Ruiz, J., Kishino, T., & Dan, B. (2014). Disruption of the LTD dialogue between the cerebellum and the cortex in Angelman syndrome model: A timing hypothesis. *Frontiers in Systems Neuroscience*, *8*, 221–230.
- Cheron, G., Prigogine, C., Cheron, J., Márquez-Ruiz, J., Traub, R. D., & Dan, B. (2014). Emergence of a 600-Hz buzz UP state Purkinje cell firing in alert mice. *Neuroscience*, *263*, 15–26.
- Cheron, G., Sausbier, M., Sausbier, U., Neuhuber, W., Ruth, P., Dan, B., & Servais, L. (2009). BK channels control cerebellar Purkinje and Golgi cell rhythmicity in vivo. *PLoS ONE*, *4*, e7991.
- Cheron, J., & Cheron, G. (2018). Beta-gamma burst stimulations of the inferior olive induce high-frequency oscillations in the deep cerebellar nuclei. *European Journal of Neuroscience*, *48*(8), 2879–2889.
- Courtemanche, R., Robinson, J. C., & Aponte, D. I. (2013). Linking oscillations in cerebellar circuits. *Frontiers in Neural Circuits*, *7*, 125–141.
- de Zeeuw, C. I., Hoebeek, F. E., Bosman, L. W. J., Schonewille, M., Witter, L., & Koekkoek, S. K. (2011). Spatiotemporal firing

- patterns in the cerebellum. *Nature Reviews. Neuroscience*, *12*, 327–344.
- de Zeeuw, C. I., Lisberger, S. G., & Raymond, J. L. (2020). Diversity and dynamism in the cerebellum. *Nature Neuroscience*, *24*(2), 160–167.
- Fernández-Vega, I., Ruiz-Ojeda, J., Juste, R. A., Geijo, M., Zarranz, J. J., Sánchez Menoyo, J. L., Vicente-Etxenausia, I., Mediavilla-García, J., & Guerra-Merino, I. (2015). Coexistence of mixed phenotype Creutzfeldt-Jakob disease, Lewy body disease and argyrophilic grain disease plus histological features of a possible Alzheimer's disease: A multi-protein disorder in an autopsy case. *The Japanese Society of Neuropathology*, *35*, 56–63.
- Fujita, H., Kodama, T., & du Lac, S. (2020). Modular output circuits of the fastigial nucleus for diverse motor and nonmotor functions of the cerebellar vermis. *eLife*, *9*, e58613.
- Gasbarri, A., Pompili, A., Pacitti, C., & Cicirata, F. (2003). Comparative effects of lesions to the ponto-cerebellar and olivocerebellar pathways on motor and spatial learning in the rat. *Neuroscience*, *116*, 1131–1140.
- Gaytán-Tocavén, L., & Olvera-Cortés, M. E. (2004). Bilateral lesion of the cerebellar-dentate nucleus impairs egocentric sequential learning but not egocentric navigation in the rat. *Neurobiology of Learning and Memory*, *82*, 120–127.
- Giovanni, A., Capone, F., di Biase, L., Ferreri, F., Florio, L., Guerra, A., Marano, M., Paolucci, M., Ranieri, F., Salomone, G., Tombini, M., Thut, G., & di Lazzaro, V. (2017). Oscillatory activities in neurological disorders of elderly: Biomarkers to target for neuromodulation. *Frontiers in Aging Neuroscience*, *9*, 189–207.
- Goedert, M. (2015). Alzheimer's and Parkinson's diseases: The prion concept in relation to assembled A $\beta$ , tau, and  $\alpha$ -synuclein. *Science*, *349*(6248), 1255555.
- Hagmeyer, S., Romão, M. A., Cristóvão, J. S., Vilella, A., Zoli, M., Gomes, C. M., & Grabrucker, A. M. (2019). Distribution and relative abundance of S100 proteins in the brain of the APP23 Alzheimer's disease model mice. *Frontiers in Neuroscience*, *13*, 640–650.
- Hansen, D. V., Hanson, J. E., & Sheng, M. (2018). Microglia in Alzheimer's disease. *The Journal of Cell Biology*, *217*, 459–472.
- He, Y., Chen, Z., Gong, G., & Evans, A. (2009). Neuronal networks in Alzheimer's disease. *The Neuroscientist: A Review Journal Bringing Neurobiology, Neurology and Psychiatry*, *15*, 333–350.
- Huth, T., Rittger, A., Saftig, P., & Alzheimer, C. (2011).  $\beta$ -Site APP-cleaving enzyme 1 (BACE1) cleaves cerebellar Na<sup>+</sup> channel  $\beta$ 4-subunit and promotes Purkinje cell firing by slowing the decay of resurgent Na<sup>+</sup> current. *Pflügers Archiv*, *461*, 355–371.
- Jacobs, H. I. L., Hopkins, D. A., Mayrhofer, H. C., Bruner, E., van Leeuwen, F. W., Raaijmakers, W., & Schmahmann, J. D. (2018). The cerebellum in Alzheimer's disease: Evaluating its role in cognitive decline. *Brain: A Journal of Neurology*, *141*, 37–47.
- Johnson, S. C., Kosciak, R. L., Jonaitis, E. M., Clark, L. R., Mueller, K. D., Berman, S. E., Bendlin, B. B., Engelman, C. D., Okonkwo, O. C., Hogan, K. J., Asthana, S., Carlsson, C. M., Hermann, B. P., & Sager, M. A. (2018). The Wisconsin registry for Alzheimer's prevention: A review of findings and current directions. *Alzheimer's & Dementia (Amsterdam, Netherlands)*, *10*, 130–142.
- Kansal, K., Yang, Z., Fishman, A. M., Sair, H. I., Ying, S. H., Jedynak, B. M., Prince, J. L., & Onyike, C. U. (2017). Structural cerebellar correlates of cognitive and motor dysfunctions in cerebellar degeneration. *Brain: A Journal of Neurology*, *140*, 707–720.
- Kelly, R. M., & Strick, P. L. (2003). Cerebellar loops with motor cortex and prefrontal cortex of a nonhuman primate. *Journal of Neuroscience: The Official Journal of the Society for Neuroscience*, *23*, 8432–8444.
- Kim, D. Y., Carey, B. W., Wang, H., Ingano, L. A. M., Binshtok, A. M., Wertz, M. H., Pettingell, W. H., He, P., Lee, V. M.-Y., Woolf, C. J., & Kovacs, D. M. (2007). BACE1 regulates voltage-gated sodium channels and neuronal activity. *Nature Cell Biology*, *9*, 755–764.
- Kovacs, D. M., Gersbacher, M. T., & Kim, D. Y. (2010). Alzheimer's secretases regulate voltage-gated sodium channels. *Neuroscience Letters*, *486*, 68–72.
- Lasn, H., Winblad, B., & Bogdanovic, N. (2001). The number of neurons in the inferior olivary nucleus in Alzheimer's disease and normal aging: A stereological study using the optical fractionator. *Journal of Alzheimer's Disease*, *3*, 159–168.
- Lasn, H., Winblad, B., & Bogdanovic, N. (2006). Neuroglia in the inferior olivary nucleus during normal aging and Alzheimer's disease. *Journal of Cellular and Molecular Medicine*, *10*, 145–156.
- Lefort, J. M., Vincent, J., Tallot, L., Jarlier, F., de Zeeuw, C. I., Rondi-Reig, L., & Rochefort, C. (2019). Impaired cerebellar Purkinje cell potentiation generates unstable spatial map orientation and inaccurate navigation. *Nature Communications*, *10*, 2251–2264.
- Lévesque, M., Gao, H., Southward, C., Langlois, J. M. P., Léna, C., & Courtemanche, R. (2020). Cerebellar cortex 4–12 Hz oscillations and unit phase relation in the awake rat. *Frontiers in Systems Neuroscience*, *14*, 475948.
- Leznik, E., & Llinás, R. (2005). Role of gap junctions in synchronized neuronal oscillations in the inferior olive. *Journal of Neurophysiology*, *94*, 2447–2456.
- Llinas, R., Baker, R., & Sotelo, C. (1974). Electrotonic coupling between neurons in cat inferior olive. *Journal of Neurophysiology*, *37*, 560–571.
- Llinás, R. R. (2013). The olivo-cerebellar system: A key to understanding the functional significance of intrinsic oscillatory brain properties. *Frontiers in Neural Circuits*, *7*, 96–109.
- Mandolesi, L., Leggio, M. G., Graziano, A., Neri, P., & Petrosini, L. (2001). Cerebellar contribution to spatial event processing: Involvement in procedural and working memory components. *The European Journal of Neuroscience*, *14*, 2011–2022.
- Márquez-Ruiz, J., & Cheron, G. (2012). Sensory stimulation-dependent plasticity in the cerebellar cortex of alert mice. *PLoS ONE*, *7*, e36184.
- Massimi, L., Pieroni, N., Maugeri, L., Fratini, M., Brun, F., Bukreeva, I., Santamaria, G., Medici, V., Poloni, T. E., Balducci, C., & Cedola, A. (2020). Assessment of plaque morphology in Alzheimer's mouse cerebellum using three-dimensional X-ray phase-based virtual histology. *Scientific Reports*, *10*(1), 11233. <https://doi.org/10.1038/s41598-020-68045-8>
- Mattsson, N., Lönneborg, A., Boccardi, M., Blennow, K., Hansson, O., & Geneva Task Force for the Roadmap of

- Alzheimer's Biomarkers. (2017). Clinical validity of cerebrospinal fluid A $\beta$ 42, tau, and phospho-tau as biomarkers for Alzheimer's disease in the context of a structured 5-phase development framework. *Neurobiology of Aging*, 52, 196–213.
- Mavroudis, I. (2019). Cerebellar pathology in Alzheimer's disease. *Hellenic Journal of Nuclear Medicine*, 22(Suppl), 174–179.
- Mavroudis, I., Petridis, F., Kazis, D., Njau, S. N., Costa, V., & Baloyannis, S. J. (2019). Purkinje cells pathology in Alzheimer's disease. *American Journal of Alzheimer's Disease and Other Dementias*, 34, 439–449.
- Mavroudis, I. A., Fotiou, D. F., Adipepe, L. F., Manani, M. G., Njau, S. D., Psaroulis, D., Costa, V. G., & Baloyannis, S. J. (2010). Morphological changes of the human purkinje cells and deposition of neuritic plaques and neurofibrillary tangles on the cerebellar cortex of Alzheimer's disease. *American Journal of Alzheimer's Disease and Other Dementias*, 25, 585–591.
- Mavroudis, I. A., Manani, M. G., Petrides, F., Petsoglou, K., Njau, S. D., Costa, V. G., & Baloyannis, S. J. (2013). Dendritic and spinal pathology of the Purkinje cells from the human cerebellar vermis in Alzheimer's disease. *Psychiatria Danubina*, 25, 221–226.
- Olivito, G., Serra, L., Marra, C., di Domenico, C., Caltagirone, C., Toniolo, S., Cercignani, M., Leggio, M., & Bozzali, M. (2020). Cerebellar dentate nucleus functional connectivity with cerebral cortex in Alzheimer's disease and memory: A seed-based approach. *Neurobiology of Aging*, 89, 32–40.
- Ordóñez-Gutiérrez, L., Antón, M., & Wandosell, F. (2015). Peripheral amyloid levels present gender differences associated with aging in A $\beta$ PP/PS1 mice. *Journal of Alzheimer's Disease*, 44, 1063–1068.
- Ordoñez-Gutiérrez, L., Fernandez-Perez, I., Herrera, J. L., Anton, M., Benito-Cuesta, I., & Wandosell, F. (2016). A $\beta$ PP/PS1 transgenic mice show sex differences in the cerebellum associated with aging. *Journal of Alzheimer's Disease*, 54, 645–656.
- Passot, J.-B., Sheynikhovich, D., Duvelle, É., & Arleo, A. (2012). Contribution of cerebellar sensorimotor adaptation to hippocampal spatial memory. *PLoS ONE*, 7, e32560.
- Person, A. L., & Raman, I. M. (2011). Purkinje neuron synchrony elicits time-locked spiking in the cerebellar nuclei. *Nature*, 481, 502–505.
- Petrosini, L., Molinari, M., & Dell'Anna, M. E. (1996). Cerebellar contribution to spatial event processing: Morris water maze and T-maze. *The European Journal of Neuroscience*, 8, 1882–1896.
- Raman, I. M., & Bean, B. P. (1997). Resurgent sodium current and action potential formation in dissociated cerebellar Purkinje neurons. *Journal of Neuroscience: The Official Journal of the Society for Neuroscience*, 17, 4517–4526.
- Raman, I. M., Gustafson, A. E., & Padgett, D. (2000). Ionic currents and spontaneous firing in neurons isolated from the cerebellar nuclei. *Journal of Neuroscience: The Official Journal of the Society for Neuroscience*, 20, 9004–9016.
- Ray, W. J., & Buggia-Prevot, V. (2020). Novel targets for Alzheimer's disease: A view beyond amyloid. *Annual Review of Medicine*, 72, 15–28.
- Rocheffort, C., Arabo, A., André, M., Poucet, B., Save, E., & Rondi-Reig, L. (2011). Cerebellum shapes hippocampal spatial code. *Science*, 334, 385–389.
- Rocheffort, C., Lefort, J. M., & Rondi-Reig, L. (2013). The cerebellum: A new key structure in the navigation system. *Frontiers in Neural Circuits*, 7, 35–47.
- Rossi, F., Wiklund, L., van der Want, J. J., & Strata, P. (1991). Reinnervation of cerebellar Purkinje cells by climbing fibres surviving a subtotal lesion of the inferior olive in the adult rat. I. Development of new collateral branches and terminal plexuses. *The Journal of Comparative Neurology*, 308, 513–535.
- Ruigrok, T. J. H., & Teune, T. M. (2014). Collateralization of cerebellar output to functionally distinct brainstem areas. A retrograde, non-fluorescent tracing study in the rat. *Frontiers in Systems Neuroscience*, 8, 23–42.
- Schmahmann, J. D. (2018). The cerebellum and cognition. *Neuroscience Letters*, 688, 62–75.
- Serenó, M. I., Diedrichsen, J., Tachrount, M., Testa-Silva, G., d'Arceuil, H., & de Zeeuw, C. (2020). The human cerebellum has almost 80% of the surface area of the neocortex. *Proceedings of the National Academy of Sciences of the United States of America*, 117, 19538–19543.
- Servais, L., Bearzatto, B., Schwaller, B., Dumont, M., de Saedeleer, C., Dan, B., Barski, J. J., Schiffmann, S. N., & Cheron, G. (2005). Mono- and dual-frequency fast cerebellar oscillation in mice lacking parvalbumin and/or calbindin D-28k. *The European Journal of Neuroscience*, 22, 861–870.
- Servais, L., & Cheron, G. (2005). Purkinje cell rhythmicity and synchronicity during modulation of fast cerebellar oscillation. *Neuroscience*, 134, 1247–1259.
- Shahnur, A., Nakano, M., Ishihara, S., Kakuda, N., Miyasaka, T., Uchiyama, H., Shirai, Y., Moniruzzaman, M., Saito, T., Saido, T. C., Nishimura, M., & Funamoto, S. (2020). A potential defense mechanism against amyloid deposition in cerebellum. *Biochemical and Biophysical Research Communications*, 535, 25–32.
- Sicot, G., Servais, L., Dinca, D. M., Leroy, A., Prigogine, C., Medja, F., Braz, S. O., Huguet-Lachon, A., Chhuon, C., Nicole, A., Gueriba, N., Oliveira, R., Dan, B., Furling, D., Swanson, M. S., Guerrera, I. C., Cheron, G., Gourdon, G., & Gomes-Pereira, M. (2017). Downregulation of the glial GLT1 glutamate transporter and purkinje cell dysfunction in a mouse model of myotonic dystrophy. *Cell Reports*, 19, 2718–2729.
- Singh-Bains, M. K., Linke, V., Austria, M. D. R., Tan, A. Y. S., Scotter, E. L., Mehrabi, N. F., Faull, R. L. M., & Dragunow, M. (2019). Altered microglia and neurovasculature in the Alzheimer's disease cerebellum. *Neurobiology of Disease*, 132, 104589.
- Stam, C. J. (2014). Modern network science of neurological disorders. *Nature Reviews. Neuroscience*, 15, 683–695.
- Sugihara, I., Lang, E. J., & Llinás, R. (1995). Serotonin modulation of inferior olivary oscillations and synchronicity: A multiple-electrode study in the rat cerebellum. *The European Journal of Neuroscience*, 7, 521–534.
- Titley, H. K., Kislin, M., Simmons, D. H., Wang, S. S.-H., & Hansel, C. (2019). Complex spike clusters and false-positive rejection in a cerebellar supervised learning rule. *The Journal of Physiology*, 597, 4387–4406.
- Uusisaari, M., & Knöpfel, T. (2008). GABAergic synaptic communication in the GABAergic and non-GABAergic cells in the deep cerebellar nuclei. *Neuroscience*, 156, 537–549.

- Vassar, R., Bennett, B. D., Babu-Khan, S., Kahn, S., Mendiaz, E. A., Denis, P., Teplow, D. B., Ross, S., Amarante, P., Loeloff, R., Luo, Y., Fisher, S., Fuller, J., Edenson, S., Lile, J., Jarosinski, M. A., Biere, A. L., Curran, E., Burgess, T., ... Citron, M. (1999).  $\beta$ -Secretase cleavage of Alzheimer's amyloid precursor protein by the transmembrane aspartic protease BACE. *Science*, *286*, 735–741.
- Watson, B. O., & Buzsáki, G. (2015). Neural syntax in mental disorders. *Biological Psychiatry*, *77*, 998–1000.
- Wegiel, J., Wisniewski, H. M., Dziwiakowski, J., Badmajew, E., Tarnawski, M., Reisberg, B., Mlodzik, B., de Leon, M. J., & Miller, D. C. (1999). Cerebellar atrophy in Alzheimer's disease-clinicopathological correlations. *Brain Research*, *818*, 41–50.
- Yu, M., Engels, M. M. A., Hillebrand, A., van Straaten, E. C. W., Gouw, A. A., Teunissen, C., van der Flier, W. M., Scheltens, P., & Stam, C. J. (2017). Selective impairment of hippocampus and posterior hub areas in Alzheimer's disease: An MEG-based multiplex network study. *Brain: A Journal of Neurology*, *140*, 1466–1485.
- Zang, Y., Hong, S., & de Schutter, E. (2020). Firing rate-dependent phase responses of Purkinje cells support transient oscillations. *eLife*, *9*, e60692.
- Zhao, R., Fowler, S. W., Chiang, A. C. A., Ji, D., & Jankowsky, J. L. (2014). Impairments in experience-dependent scaling and stability of hippocampal place fields limit spatial learning in a mouse model of Alzheimer's disease. *Hippocampus*, *24*, 963–978.
- Zhou, H., Lin, Z., Voges, K., Ju, C., Gao, Z., Bosman, L. W. J., Ruigrok, T. J. H., Hoebeek, F. E., de Zeeuw, C. I., & Schonewille, M. (2014). Cerebellar modules operate at different frequencies. *eLife*, *3*, e02536.
- Zott, B., Simon, M. M., Hong, W., Unger, F., Chen-Engerer, H.-J., Frosch, M. P., Sakmann, B., Walsh, D. M., & Konnerth, A. (2019). A vicious cycle of  $\beta$  amyloid-dependent neuronal hyperactivation. *Science*, *365*, 559–565.

**How to cite this article:** Cheron, G., Ristori, D., Marquez-Ruiz, J., Cebolla, A.-M., & Ris, L. (2022). Electrophysiological alterations of the Purkinje cells and deep cerebellar neurons in a mouse model of Alzheimer disease (electrophysiology on cerebellum of AD mice). *European Journal of Neuroscience*, 1–17. <https://doi.org/10.1111/ejn.15621>